Distilling the Past: Information-Dense and Style-Aware Replay for Lifelong Person Re-Identification

Mingyu Wang[1], Wei Jiang[1*], Haojie Liu[1], Zhiyong Li[1], Q. M. Jonathan Wu[2]

[1*]College of Control Science and Engineering, Zhejiang University, Hangzhou, China.
[2]Department of Electrical and Computer Engineering, University of Windsor, Canada.

*Corresponding author(s). E-mail(s): jiangwei_zju@zju.edu.cn;
Contributing authors: wangmingyu@zju.edu.cn; liuhaojie@zju.edu.cn;
lizhiyong_zju@zju.edu.cn; jwu@uwindsor.ca;

Abstract

Lifelong person re-identification (LReID) aims to continuously adapt to new domains while mitigating catastrophic forgetting. While replay-based methods effectively alleviate forgetting, they are constrained by strict memory budgets, leading to limited sample diversity. Conversely, exemplar-free approaches bypass memory constraints entirely but struggle to preserve the fine-grained identity semantics crucial for Re-ID tasks. To resolve this fundamental dilemma, we propose an Information-Dense and Style-Aware Replay framework. Instead of storing a sparse set of raw historical images, we fuse the knowledge of sequential data into the pixel space of a compact replay buffer via multi-stage gradient matching and identity supervision. This condensation process not only maximizes the semantic representativeness of limited memory but also naturally conceals original visual details, inherently preserving data privacy. Furthermore, to combat forgetting induced by cross-domain shifts, we introduce a dual-alignment style replay strategy that adapts both current and fused replay samples, harmonizing feature representations across disparate domains. Extensive experiments on multiple LReID benchmarks demonstrate that our method significantly outperforms existing approaches, achieving improvements of +5.0% and +6.0% in Seen-Avg mAP over current state-of-the-art and traditional replay-based methods, respectively, thereby establishing an efficient and robust new baseline for lifelong learning.

Keywords: Person Re-identification, Information Fusion, Style Alignment, Lifelong Learning

1 Introduction

Person re-identification (Re-ID) has achieved remarkable progress in recent years, largely driven by the assumption of static, single-domain data distributions. However, in real-world applications, data streams are typically dynamic and continuously evolve over time [1]. Training a model jointly on all historical data is often computationally prohibitive and practically infeasible. This limitation has motivated the emergence of Lifelong Person Re-identification (LReID), which requires a model to continuously adapt to new domains without severely degrading its performance on previously learned ones—a challenge widely known as catastrophic forgetting [2].

To mitigate catastrophic forgetting, recent literature primarily explores two directions: replay-based and exemplar-free methods. Replay-based approaches [3] explicitly store a small subset

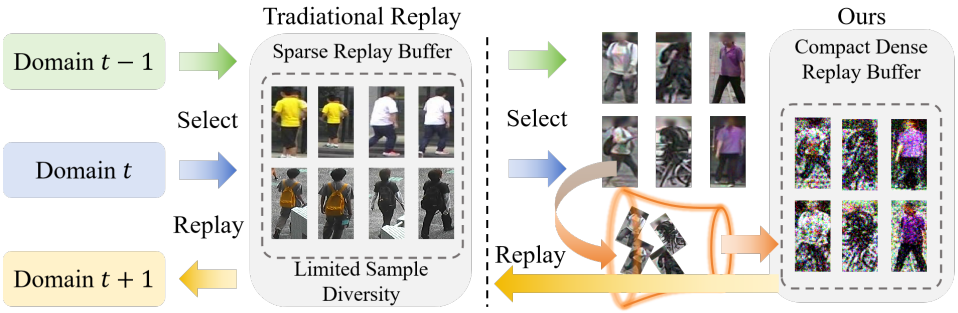

Fig. 1: Instead of storing sparse raw images, our **Information-Dense Replay** condenses multiple samples into a single representation via pixel-level optimization, breaking physical memory bottlenecks.

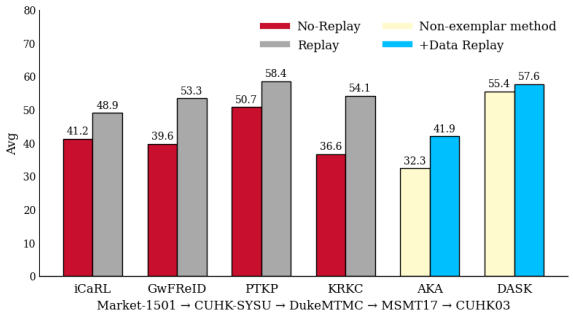

Fig. 2: Performance comparison of different methods. We observe that incorporating data replay consistently improves performance, regardless of whether the method initially relies on it, highlighting its effectiveness in LReID scenarios.

of historical samples in an auxiliary memory buffer and rehearse them during current domain training. While straightforward and effective, these methods are fundamentally bottlenecked by strict memory budgets, resulting in severely limited sample diversity. Furthermore, storing raw personal images inevitably raises potential privacy concerns. Because Re-ID datasets consist of surveillance images of real pedestrians, the unauthorized retention of their raw biometric data poses a significant risk of portrait rights infringement. In the event of a compromised server, a malicious entity with full access to this raw memory buffer could easily execute Data Reconstruction or Membership Inference Attacks (MIA) to extract sensitive biometric identifiers (e.g., high-frequency facial details) or deduce an individual's presence in the historical training data. In contrast, exemplar-free methods, encompassing techniques like knowledge distillation [4] and distribution rehearsing [5], attempt to bypass physical memory constraints entirely. Specifically, distribution rehearsing methods aim to capture historical domain styles or replay abstract distribution statistics. However, because person Re-ID inherently relies on high-dimensional, fine-grained identity features, relying solely on abstract statistics inevitably sacrifices crucial identity semantics. This semantic loss ultimately leads to a precipitous drop in performance on older domains over time. Indeed, as illustrated in Figure 2, incorporating data replay consistently improves performance across various baselines, highlighting its indispensability for LReID scenarios. This creates a challenging dilemma: how can we preserve rich, fine-grained historical knowledge under strict memory and data privacy constraints?

To break this bottleneck, we shift our perspective from discrete sample selection to continuous information condensation. Rather than debating which few raw images to keep, we ask: *can we fuse the knowledge of multiple historical images into a single synthetic representation?* Motivated by this, we propose an Information-Dense Replay framework based on dataset distillation. Instead of storing a sparse set of original images, we condense the sequential data into a compact replay buffer via multi-stage gradient matching and identity supervision. By optimizing the synthetic samples at the pixel level, we ensure they provide similar parameter updates to the network as the original dataset. This process drastically maximizes the semantic representativeness and information density of the limited memory. As a highly desirable by-product, this condensation process naturally distorts original visual details, implicitly preserving data privacy without requiring complex manual masking heuristics (as illustrated in Figure 1).

However, simply retaining dense historical content is insufficient, as the severe domain shift between old and new tasks remains another primary catalyst for forgetting in LReID. To bridge this gap, we further introduce a Dual-Alignment Style Replay strategy. Capitalizing on our synthetic, privacy-friendly replay samples, we train a transformation network guided by both deep and shallow matching constraints. This network is then utilized to perform bidirectional stylization: it injects previous domain styles into current domain features, while simultaneously transferring the new domain style to the fused replay samples. By jointly training on these harmonized hybrid representations, our model effectively aligns feature spaces across disparate domains, neutralizing the negative impact of cross-domain style variations.

The main contributions of this paper are summarized as follows:

- We propose a novel Information-Dense Replay paradigm for LReID. By utilizing pixel-level multi-stage gradient matching, we fuse knowledge from multiple images into a compact buffer, breaking the physical memory bottleneck while inherently providing privacy protection.
- We introduce a Dual-Alignment Style Replay strategy that bidirectionally adapts both current data and fused replay samples, significantly mitigating catastrophic forgetting caused by cross-domain style shifts.
- Extensive experiments on multiple LReID benchmarks demonstrate that our method establishes a new state-of-the-art. Notably, its average performance across forgetting mitigation and generalization metrics closely approaches the theoretical upper bound of joint training, despite strictly limited data access.

2 Related Works

2.1 Person Re-Identification

Person Re-Identification (Re-ID) aims to retrieve images of a specific identity across non-overlapping camera networks [6]. Extensive research has driven remarkable progress in standard image-based [7, 8], video-based [9, 10], and cross-modality scenarios [11, 12]. However, these traditional paradigms heavily rely on the assumption of static datasets and offline joint training. In practical deployments, data streams are dynamic and continuously evolving [13, 14], which renders retraining from scratch computationally prohibitive and impractical [15, 16]. This gap has motivated the shift towards Lifelong Person Re-Identification (LReID) [2], which requires models to incrementally adapt to dynamically changing data distributions. Furthermore, real-world deployments increasingly demand both efficiency and data privacy. While existing attempts to manage sensitive data often rely on heavy encryption schemes [17] or user-specific keys [18], these methods introduce severe computational overhead, making them unsuitable for LReID scenarios. In contrast, our proposed information-dense strategy fundamentally optimizes memory efficiency, naturally avoiding these overheads and yielding data protection as a free by-product.

2.2 Lifelong Person Re-Identification

LReID requires a model to sequentially adapt to new domains without suffering from catastrophic forgetting of previously acquired knowledge [2, 19]. Existing strategies to mitigate forgetting primarily fall into exemplar-free and replay-based paradigms.

Exemplar-free methods, encompassing knowledge distillation [20–22] and distribution rehearsing [5, 23], aim to transfer historical knowledge without explicitly storing past images. Specifically, knowledge distillation achieves this by aligning the output probabilities or intermediate feature representations of a frozen historical model with those of the new model being updated. Meanwhile, distribution rehearsing reconstructs past feature spaces using auxiliary networks to bridge the gap between current and historical domains. While these methods naturally circumvent memory constraints and privacy risks, they struggle in the Re-ID domain. Because Re-ID inherently relies on extremely fine-grained identity semantics, continuously updating model parameters via distillation or relying solely on replayed abstract distributions inevitably leads to the gradual loss of specific identity features over time.

Conversely, data replay strategies [3, 24] maintain a small memory buffer of past raw samples for

joint training. While highly effective at preserving precise semantic details, these methods are fundamentally bottlenecked by strict memory budgets, resulting in severely sparse sample diversity. Additionally, storing raw personal images raises significant privacy concerns. In this work, we bridge the gap between these two paradigms by proposing a novel framework that fuses dense historical information into synthetic samples, maintaining fine-grained semantics without bounded memory limits or raw data storage.

2.3 Dataset Distillation

Dataset Distillation (DD) aims to condense the rich knowledge of large-scale datasets into a significantly smaller set of synthetic samples while maintaining comparable training efficacy.

Current DD approaches typically achieve this by aligning training dynamics, such as gradients [25, 26], feature distributions [27], or training trajectories [28]. Beyond standard classification, DD has recently been introduced to Continual Learning to summarize streaming data under strict memory constraints [29]. Simultaneously, because its pixel-level optimization naturally distorts original visual semantics, DD has also been explored as a tool for privacy preservation [30, 31]. However, existing DD-based CL methods primarily target coarse-grained tasks and struggle to preserve the fine-grained identity features essential for Re-ID. Meanwhile, existing privacy-driven DD methods often introduce complex optimization loops that are too computationally heavy for dynamic lifelong scenarios.

To address these limitations, we introduce a novel distillation-based replay paradigm tailored specifically for LReID. By utilizing multi-stage gradient matching and identity supervision, our method effectively fuses the sequential historical knowledge into a highly compact buffer. This approach breaks the physical memory bottleneck to provide an Information-Dense Replay that preserves crucial fine-grained semantics. Furthermore, it naturally leverages the visual distortion of the condensation process, achieving robust data privacy as a computationally free by-product without slowing down the lifelong learning process.

3 Preliminaries

3.1 Background on Dataset Distillation

The general goal of DD is to generate a small synthetic dataset $\mathcal{S} = \{(x_i, y_i)\}_{i=1}^{N_S}$ from a large-scale dataset $\mathcal{T} = \{(x_i, y_i)\}_{i=1}^{N_T}$, where the synthetic data retains the most critical training information from the original data. Here, each x_i denotes an image with a corresponding class label y_i, and $N_S \ll N_T$.

The ultimate purpose of DD is to synthesize a compact set of data that enables models trained on it to achieve comparable performance to those trained on the full dataset. Formally, the objective of DD can be formulated as minimizing the performance gap on the original evaluation set between models trained on the synthetic data and those trained on the full dataset:

$$\min_{\mathcal{S}} \mathbb{E}_{(x,y)\sim\mathcal{T}} \left[\left| \ell\left(\phi_{\theta_\mathcal{T}}(x), y\right) - \ell\left(\phi_{\theta_\mathcal{S}}(x), y\right) \right| \right], \quad (1)$$

where $\ell(\cdot,\cdot)$ and θ represent the loss function and the parameters of the network, respectively.

However, solving Eq. 1 naively requires inner-loop network retraining each time $\mathcal{S}$ is updated, which is computationally prohibitive. Therefore, existing methods attempt to avoid repeated training loops by introducing surrogate objectives. In this way, the optimal synthetic dataset $\mathcal{S}^*$ can be obtained by optimizing:

$$\mathcal{S}^* = \arg\min_{\mathcal{S}} \mathbb{E}_\theta[\ell(\psi(\mathcal{T};\theta), \psi(\mathcal{S};\theta))], \quad (2)$$

where ψ denotes a surrogate matching objective, such as gradients or distribution statistics.

In this work, we adopt gradient matching as our core objective but adapt it for the dynamic LReID setting via a multi-stage matching strategy. Rather than merely reducing the dataset size, our primary goal is to maximize the semantic information density of the limited replay buffer. As a highly desirable by-product, this pixel-level optimization naturally distorts the original visual semantics, inherently safeguarding data privacy without requiring additional constraints.

3.2 Replay-based LReID

In this work, we focus on the LReID setting. We consider a sequence of T tasks $\mathcal{D} = \{\mathcal{D}_t\}_{t=1}^{T}$, where each task $\mathcal{D}_t = \{(x_t^i, y_t^i)\}_{i=1}^{n_t}$ contains n_t pairs of data samples and identity labels. At each training step t, the model is only allowed to access the current task $\mathcal{D}_t$, while previous tasks $\{\mathcal{D}_1, \ldots, \mathcal{D}_{t-1}\}$ are no longer accessible. After training on task t, the model is evaluated on a set of t test datasets $\mathcal{D}^{\mathrm{e}} = \{\mathcal{D}_1^{\mathrm{e}}, \ldots, \mathcal{D}_t^{\mathrm{e}}\}$, each corresponding to a previously seen training domain. The objective of LReID is to maximize the overall identification accuracy across all seen tasks.

To tackle the challenge of catastrophic forgetting, replay-based methods maintain a small auxiliary memory $\mathcal{M} = \{(x_m, y_m)\}_{m=1}^{N}$ to store representative samples from previous tasks, where N denotes the strict memory size limit. As illustrated in Figure 1, instead of populating $\mathcal{M}$ with sparse raw images, we condense sequential data and fuse multiple original samples (x_m, y_m) into a single synthetic image $(\tilde{x}_m, \tilde{y}_m)$ to construct an information-dense memory $\tilde{\mathcal{M}}$.

During each iteration of the current task, a batch $\tilde{\mathcal{B}}_m = \{(\tilde{x}_m^i, \tilde{y}_m^i)\}_{i=1}^{B_m}$ is sampled from this condensed memory and jointly trained with the current batch $\mathcal{B}_t = \{(x_t^i, y_t^i)\}_{i=1}^{B_t}$. The joint training process is formulated as follows:

$$\theta^* = \arg\min_{\theta} \mathcal{L}\left(\theta; \mathcal{B}_t\right) + \lambda \mathcal{L}_r\left(\theta; \tilde{\mathcal{B}}_m\right), \quad (3)$$

where θ denotes the model parameters, $\mathcal{L}(\cdot;\cdot)$ is the training objective for the current task, $\mathcal{L}_r(\cdot;\cdot)$ is the objective for data replay, and λ is a balancing coefficient.

While accessing previous domains effectively mitigates cross-domain forgetting, traditional methods limit the memory $\mathcal{M}$ to raw images. This fundamentally restricts sample diversity under bounded memory and inevitably raises privacy concerns, causing some approaches to abandon replay entirely (which severely degrades performance, as shown in Figure 2). By constructing the synthetic memory $\tilde{\mathcal{M}}$, our method breaks physical memory constraints to retain rich historical semantics, successfully re-enabling powerful data replay in privacy-sensitive LReID scenarios.

4 Method

4.1 Information-Dense Data Replay

The primary objective of this section is to synthesize a highly compact and information-dense replay buffer $\mathcal{S}$ from the original sequential data $\mathcal{T}$. Instead of explicitly storing a sparse set of raw pedestrian images, which inherently incurs strict memory bottlenecks and limits sample diversity, we optimize synthetic samples at the pixel level to encapsulate the rich training dynamics of the original dataset. By jointly training on this fused replay data and the current domain data, the model continuously adapts while effectively mitigating catastrophic forgetting. Furthermore, this extreme condensation process naturally distorts original visual details, inherently providing data privacy without requiring complex cryptographic mechanisms. The overall pipeline of our proposed method is illustrated in Figure 3.

Privacy-Guided Initialization via Region Masking. To establish a fundamental baseline for privacy protection, we apply region-wise obfuscation to the synthetic samples before the condensation process begins. Specifically, we target facial regions, which contain the highest concentration of sensitive biometric identifiers. Given an initial image x_i, we define a fixed proportional region of interest (ROI) covering the facial area and apply a Gaussian blur to aggressively distort high-frequency details. Because these blurred initialization samples are subsequently optimized through multi-stage pixel-level condensation, the superficial loss of visual information does not degrade the underlying structural and semantic knowledge transferred during gradient matching.

Information-Dense Condensation via Gradient Matching. The core mechanism of our proposed method relies on DD principles to maximize memory efficiency. Our goal is to synthesize an information-dense buffer $\mathcal{S}$ that elicits similar parameter updates to the network as the full original dataset $\mathcal{T}$. Formally, let $\theta_k^{\mathcal{S}}$ and $\theta_k^{\mathcal{T}}$ denote the model parameters at training step k optimized on the synthetic and real datasets, respectively. We aim to minimize the parameter distance at the end of K training steps:

$$\min_{\mathcal{S}} \mathbb{E}_{\theta_0}\left[\mathcal{D}(\theta_K^{\mathcal{S}}, \theta_K^{\mathcal{T}})\right], \quad (4)$$

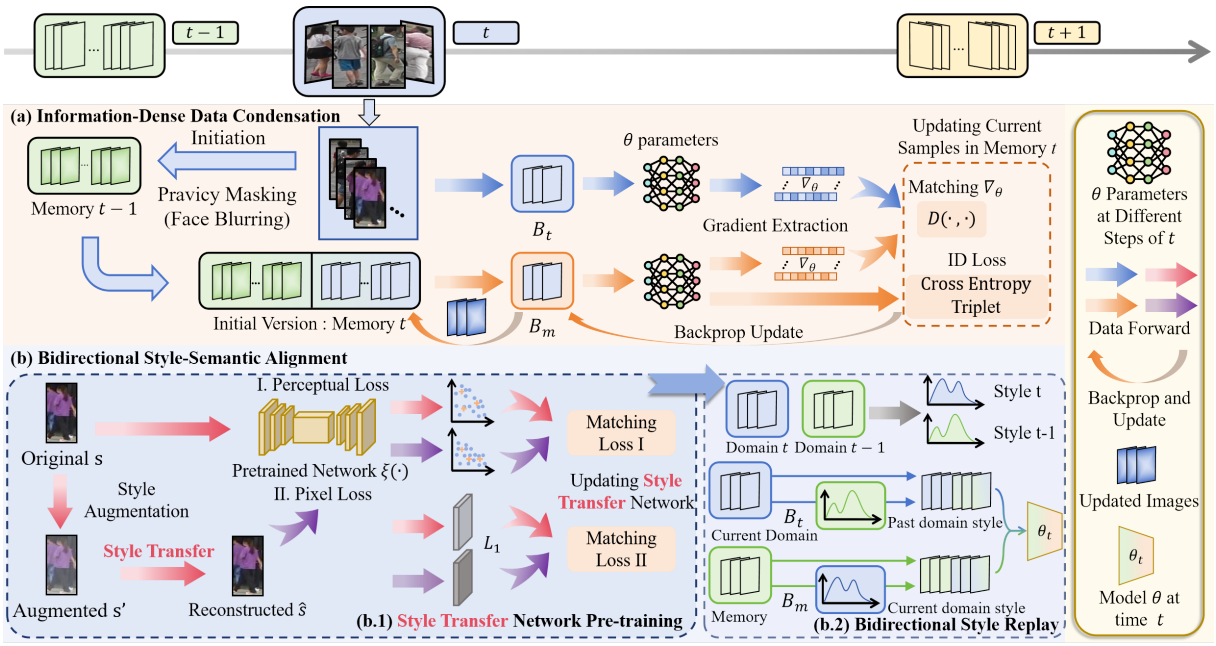

Fig. 3: **Overall pipeline of our proposed framework. (a) Information-Dense Data Condensation:** During the training phase on domain D_t, informative replay samples are generated by aligning their gradients with the original data across multiple parameter stages, guided by the ID loss. **(b) Bidirectional Style-Semantic Alignment:** To mitigate catastrophic forgetting induced by domain shifts, we introduce a dual-alignment mechanism. **(b.1)** A style transfer network is pre-trained under the supervision of pixel and perceptual reconstruction losses. **(b.2)** During joint optimization on domain D_{t+1}, style transfer is applied bidirectionally—injecting past styles into current streaming data and current styles into buffered replay samples, ensuring robust representation learning across domains.

where $\mathcal{D}(\cdot,\cdot)$ denotes a distance metric and θ_0 is the shared initialization. Unrolling the training process, the parameters update via standard gradient descent:

$$\begin{aligned}\theta_k^{\mathcal{S}} &= \theta_{k-1}^{\mathcal{S}} - \eta\nabla_\theta\mathcal{L}^{\mathcal{S}}(\theta_{k-1}^{\mathcal{S}}),\\ \theta_k^{\mathcal{T}} &= \theta_{k-1}^{\mathcal{T}} - \eta\nabla_\theta\mathcal{L}^{\mathcal{T}}(\theta_{k-1}^{\mathcal{T}}),\end{aligned} \tag{5}$$

where η is the learning rate. Directly optimizing Eq. 4 requires unrolling the entire computational graph through all K steps, which is highly memory-intensive and computationally prohibitive. To make this tractable, we derive a surrogate objective based on the recursive expansion of the parameter discrepancy.

Let $\Delta\theta_k = \theta_k^{\mathcal{S}} - \theta_k^{\mathcal{T}}$ denote the parameter discrepancy at step k. Assuming both models start from the same initialization ($\Delta\theta_0 = 0$), the parameter difference at step k can be expanded recursively:

$$\Delta\theta_k = \Delta\theta_{k-1} - \eta\left(\nabla_\theta\mathcal{L}^{\mathcal{S}}(\theta_{k-1}^{\mathcal{S}}) - \nabla_\theta\mathcal{L}^{\mathcal{T}}(\theta_{k-1}^{\mathcal{T}})\right).$$

By unrolling this recurrence relation from step 0 to K, we obtain the accumulated discrepancy:

$$\Delta\theta_K = -\eta\sum_{i=0}^{K-1}\left(\nabla_\theta\mathcal{L}^{\mathcal{S}}(\theta_i^{\mathcal{S}}) - \nabla_\theta\mathcal{L}^{\mathcal{T}}(\theta_i^{\mathcal{T}})\right).$$

Applying the triangle inequality, the norm of the parameter distance $\|\Delta\theta_K\|$ is strictly bounded by the sum of the gradient distances:

$$\|\Delta\theta_K\| \le \eta\sum_{i=0}^{K-1}\left\|\nabla_\theta\mathcal{L}^{\mathcal{S}}(\theta_i^{\mathcal{S}}) - \nabla_\theta\mathcal{L}^{\mathcal{T}}(\theta_i^{\mathcal{T}})\right\|. \tag{6}$$

Under the assumption of local linearity and Lipschitz continuous loss landscapes, strictly minimizing the step-wise gradient discrepancy acts as a rigorous surrogate upper bound for minimizing the final parameter distance.

Trajectory-Matching Approximation. While Eq. 6 simplifies the objective, dynamically computing the coupled states $\theta_i^{\mathcal{S}}$ and $\theta_i^{\mathcal{T}}$ at every

step still necessitates inner-loop unrolling. To circumvent this, we introduce a trajectory-matching approximation. If the gradient matching is successful at each preceding step i, we can reliably assume that the synthetic trajectory closely follows the real trajectory, i.e., $\theta_i^{\mathcal{S}} \approx \theta_i^{\mathcal{T}}$. This critical assumption allows us to decouple the trajectories and evaluate both gradients at the identical, precomputed network state of the real data, denoted as $\tilde{\theta}_i^{\mathcal{T}}$.

During the initial training on the real domain, we save the model parameters at selected intermediate stages, forming a discrete expert trajectory set $\{\tilde{\theta}_t^{\mathcal{T}} \mid t \in \mathcal{T}_s\}$, where $\mathcal{T}_s$ consists of evenly spaced epochs designed to capture diverse optimization phases (e.g., early rapid convergence and late-stage refinement). By fixing the network state to these pre-saved anchor points, we force the synthetic data to reproduce the exact gradient direction of the real data at multiple critical states. The final, computationally efficient gradient matching objective is thus reformulated as:

$$\mathcal{L}_{grad} = \mathbb{E}_{t\in\mathcal{T}_s}\left[\mathcal{D}_{cos}\left(\nabla_\theta \mathcal{L}^{\mathcal{S}}(\tilde{\theta}_t^{\mathcal{T}}), \nabla_\theta \mathcal{L}^{\mathcal{T}}(\tilde{\theta}_t^{\mathcal{T}})\right)\right], \tag{7}$$

where $\mathcal{D}_{cos}$ denotes the cosine distance, ensuring directional alignment of the optimization trajectories regardless of gradient magnitude scaling.

Semantic Preservation via Identity Supervision. While Eq. 7 effectively captures global training dynamics, a fundamental limitation arises in fine-grained tasks like person Re-ID: gradient matching alone focuses on averaged batch-level trajectories, often leading to feature collapse where inter-class margins are blurred. To preserve the strict intra-class compactness and inter-class separability required for Re-ID, we introduce explicit Identity Supervision (ID Loss) as a semantic regularizer during the pixel-level condensation.

This supervision ensures that the highly compressed pixels retain discriminative abstract identity manifolds. The identity supervision consists of a cross-entropy loss $\mathcal{L}_c$ and a triplet loss $\mathcal{L}_t$. The classification loss is formulated as:

$$\mathcal{L}_c = -\frac{1}{N}\sum_{i=1}^{N}\log\left(\frac{\exp(s_{i,y_i})}{\sum_{j=1}^{C}\exp(s_{i,j})}\right), \tag{8}$$

where N is the batch size, C is the number of identities, $s_{i,j}$ is the predicted logit, and y_i is the ground-truth label. To explicitly constrain the fine-grained metric space, we apply the hardest-sample triplet loss:

$$\mathcal{L}_t = \frac{1}{N}\sum_{i=1}^{N}\log\left(1+\exp\left(d_{ap}^{(i)} - d_{an}^{(i)}\right)\right), \tag{9}$$

where $d_{ap}^{(i)}$ and $d_{an}^{(i)}$ denote the maximum intra-class and minimum inter-class feature distances for anchor i, respectively.

The final comprehensive loss used to continuously update the pixels of the synthetic replay buffer $\mathcal{S}$ is defined as:

$$\mathcal{L}_{total} = \alpha \cdot \mathcal{L}_{grad} + (\mathcal{L}_c + \mathcal{L}_t), \tag{10}$$

where α is a balancing hyperparameter. Guided by $\mathcal{L}_{total}$, the synthetic samples iteratively absorb dense structural information and decision boundaries from the real dataset. This multi-objective optimization produces a memory-efficient buffer that strictly enhances replay effectiveness while intrinsically masking sensitive raw data.

4.2 Bidirectional Style-Semantic Alignment

During the replay phase, we train the model using both current-domain samples and buffered replay samples. However, the replay memory contains samples from multiple past domains, and the domain shift can hinder effective training. While some non-exemplar methods like DASK and CoP address domain shifts via style transfer, they rely solely on pixel-level L1 reconstruction losses. For fine-grained tasks like person Re-ID, simply using L1 loss can smooth out high-frequency structural details (e.g., textures, edges) that are critical for retrieval.To solve this, we propose Bidirectional Style-Semantic Alignment (BSSA). We perform a dual-translation process: we apply historical domain styles to the current streaming data, and we inject current domain styles into the replay buffer samples. This bidirectional translation allows the model to observe the same content under different domain styles, reducing the negative impact of domain shifts.

Style Augmentation and Transfer. Given an input sample s, we first apply channel-wise style augmentation. We compute the augmented mean

μ_r and standard deviation σ_r by randomly sampling a batch from the current dataset. This simulates various domain-specific style distributions. Then, we pass the augmented input s' through a lightweight style transfer module to produce the reconstructed output $\hat{s}$.

Perceptual Integrity Safeguard. Existing methods optimize style transfer primarily using the pixel-level loss, $\mathcal{L}_{\text{L1}} = \|\hat{s} - s\|_1$. However, from a spatial frequency perspective, pixel-wise losses implicitly prioritize low-frequency signals (e.g., global color and illumination). Because predicting exact high-frequency structural alignments under domain shifts incurs heavy spatial penalties, the network tends to output smoothed, averaged pixel values to minimize the expected $L1$ error. Consequently, crucial high-frequency identity cues (e.g., distinct patterns, edge boundaries) are irrecoverably blurred.To bound this structural divergence, we constrain the optimization in a spatial gradient space rather than the raw pixel space. We map the images into a deep feature space using a fixed pretrained network, denoted as $\xi(\cdot)$. Since early convolutional layers function as non-linear spatial filters that extract local gradients, the feature map $\xi(s)$ explicitly encodes the high-frequency structural geometry of the image. By enforcing a constraint in this feature space, we guarantee that the identity-specific structural features are preserved even as the low-frequency style shifts. The perceptual loss is thus defined as:

$$\mathcal{L}_{\text{perc}} = \|\xi(\hat{s}) - \xi(s)\|_2^2 \tag{11}$$

This safeguard ensures the model alters the superficial domain style without morphing the structural identity. The total style reconstruction objective combines the pixel-wise L1 loss and the perceptual loss:

$$\mathcal{L}_{\text{total}} = \mathcal{L}_{\text{L1}} + \beta \mathcal{L}_{\text{perc}} \tag{12}$$

where β is the weight for the structural constraint.

Joint Optimization. Finally, we integrate these stylistically aligned samples into the training process. The overall objective function for the current task is:

Algorithm 1 Information-Dense and Style-Aware Replay

Input: Current task D_t, memory $\mathcal{M}$, replay data $\mathcal{S} \subset \mathcal{M}$
Required: Model parameters θ trained on domain $t-1$; number of update steps Z; learning rates for LReID model weights γ, λ, and synthetic samples η_S
Initialize: Apply image masking to samples from domain t stored in memory $\mathcal{M}$

1: **for** $z = 0$ **to** $Z - 1$ **do**
2: Sample mini-batch $\mathcal{B}_t^c \sim D_t$ and $\mathcal{B}_m^c \sim \mathcal{M}$, both from class c
3: Calculate loss $\mathcal{L}_S$ by Eqs. 7, 8, 9, and 10
4: Update synthetic samples: $\mathcal{S} \leftarrow \mathcal{S} - \eta_S \nabla_\theta \mathcal{L}_S$
5: **end for**
6: Apply style transfer to both current domain samples and replay samples
7: Calculate overall loss by Eq. 13:
$$\mathcal{L} = \mathcal{L}(\theta; \mathcal{B}_t) + \gamma \mathcal{L}(\theta; \mathcal{B}_t') + \lambda\big(\mathcal{L}_r(\theta; \tilde{\mathcal{B}}_m) + \gamma\, \mathcal{L}_r(\theta; \tilde{\mathcal{B}}_m')\big)$$
8: Update model parameters:
$$\theta \leftarrow \theta - \nabla_\theta \mathcal{L} - \gamma \nabla_\theta \mathcal{L} - \lambda \nabla_\theta \mathcal{L}_r$$

Ensure: Updated model θ_t, updated memory $\mathcal{M}$

$$\theta^* = \arg\min_\theta \Big\{ \mathcal{L}(\theta; \mathcal{B}_t) + \gamma\, \mathcal{L}(\theta; \mathcal{B}_t') + \lambda\big(\mathcal{L}_r(\theta; \tilde{\mathcal{B}}_m) + \gamma\, \mathcal{L}_r(\theta; \tilde{\mathcal{B}}_m')\big) \Big\} \tag{13}$$

where $\mathcal{B}_t$ and $\mathcal{B}_t'$ represent the current task batch before and after style transfer, respectively. Similarly, $\tilde{\mathcal{B}}_m$ and $\tilde{\mathcal{B}}_m'$ are the replay batch before and after style transfer. The parameters γ and λ are weighting coefficients. Following prior works in LReID, the loss functions $\mathcal{L}$ and $\mathcal{L}_r$ consist of a Triplet Loss and a Cross-Entropy Loss.

5 Experiments

5.1 Benchmarks and Evaluation Metrics

Benchmarks. We conduct all experiments on the LReID benchmark, which consists of five ReID datasets: Market1501 [32], DukeMTMC [33],

Table 1: Dataset statistics under original and LReID settings.

Type	Datasets	Original Identities			LReID Identities		
		Train	Query	Gallery	Train	Query	Gallery
Replay	CUHK03	767	700	700	500	700	700
	Market-1501	751	750	751	500	751	751
	DukeMTMC	702	702	1110	500	702	1110
	CUHK-SYSU	942	2900	2900	500	2900	2900
	MSMT17	1041	3060	3060	500	3060	3060
Unseen Domains	i-LIDS	243	60	60	-	60	60
	VIPeR	316	316	316	-	316	316
	GRID	125	125	126	-	125	126
	PRID	100	100	649	-	100	649
	CUHK01	485	486	486	-	486	486
	CUHK02	1677	239	239	-	239	239
	SenseReID	1718	521	1718	-	521	1718

CUHK-SYSU [34], MSMT17-V2 [35], and CUHK03 [36]. Following previous work [2], we adopt two training orders to simulate various lifelong learning scenarios.[1] [2] In addition to the training datasets, we further evaluate the model on seven unseen ReID datasets (CUHK01 [37], CUHK02 [38], VIPeR [39], PRID [40], iLIDS [41], GRID [42] and SenseReID [43]) to assess its generalization ability.

Detailed Overview of LReID Benchmarks. To ensure a fair comparison, we follow the settings proposed by [2, 5], adopting two types of LReID benchmarks. The detailed statistics are presented in Table 1. Both benchmarks consist of 12 existing ReID datasets, differing only in the order of domain training. Here, *Original Identities denotes* the number of identities in the original datasets, while *LReID Identities* refers to the selected subset used in the LReID benchmark.

For the CUHK-SYSU dataset, we follow the preprocessing method of [2], where ground-truth person bounding box annotations are used to crop individual person images. We then select a subset in which each identity contains at least four bounding boxes. In the LReID benchmark, the number of *LReID Identities* is set to 500 for each training domain to ensure identity-balanced conditions.

Evaluation Protocol. We use mean Average Precision (mAP) and Rank-1 accuracy (R@1) on each dataset to evaluate the model's performance on specific domains. Furthermore, the average mAP and average R@1 across all training (seen) and unseen domains are calculated to evaluate the model's resistance to forgetting and its overall generalization ability in the lifelong learning setting.

[1] Train Order 1: Market-1501 → CUHK-SYSU → DukeMTMC → MSMT17 → CUHK03

[2] Train Order 2: DukeMTMC → MSMT17 → Market-1501 → CUHK-SYSU → CUHK03

5.2 Implementation Details

To ensure a fair and rigorous comparison with existing literature, we adopt ResNet-50 as the feature extraction backbone for our Re-ID model. For the style transfer module, following established practices [5], we employ AKPNet built upon a MobileNetV3 [44] architecture. During the training phase, a standard ResNet-50 network is utilized to extract features and compute the matching gradients.

Regarding the training schedule, the synthetic samples in the replay buffer are optimized for 3 epochs during the condensation phase, while the style transfer network is trained for 50 epochs per dataset. For the lifelong Re-ID process across both task sequences (orders), the model is trained for 80 epochs on the initial base domain and 60 epochs on each subsequent domain. All input images are resized to 256×128 pixels and augmented using random cropping, random erasing, and horizontal flipping. The training batch size is set to 128, formulated by randomly sampling 32 identities with 4 images per identity. The Re-ID model is optimized using SGD with an initial learning rate of 0.008 and a weight decay of 0.0001. The loss balancing hyperparameters γ and λ are set to 4.5 and 1.0, respectively. For the pixel-level optimization of the synthetic replay samples, we utilize SGD with a learning rate of 0.002 and a momentum of 0.9, and the gradient matching coefficient α is empirically set to 0.01. All experiments are implemented using the PyTorch framework and executed on two NVIDIA RTX 4090 GPUs.

5.3 Comparison with State-of-the-art Methods

We compare the proposed method with three categories of methods: (1) Class-Incremental Learning methods (CIL), including LwF [45], SPD [46], PRAKA [47] and FCS [48]; (2) Replay-based methods (KRKC [3]); and (3) Non-exemplar

Table 2: Comparison of different methods on Training Order-1 with mAP and R1 scores. Best results are highlighted in deep lavender and second best in light lavender.

	Method	Publication	Market-1501		CUHK-SYSU		DukeMTMC		MSMT17		CUHK03		Seen-Avg		UnSeen-Avg	
			mAP	R@1	mAP	R@1	mAP	R@1	mAP	R@1	mAP	R@1	mAP	R@1	mAP	R@1
	JointTrain	-	78.9	90.9	86.7	88.2	71.2	82.9	36.2	61.2	61.2	63.4	66.8	77.3	59.4	52.6
CIL	LwF	TPAMI 2017	56.3	77.1	72.9	75.1	29.6	46.5	6.0	16.6	36.1	37.5	40.2	50.6	47.2	42.6
CIL	SPD	ICCV 2019	35.6	61.2	61.7	64.0	27.5	47.1	5.2	15.5	42.2	44.3	34.4	46.4	40.4	36.6
CIL	PRAKA	ICCV 2023	37.4	61.3	69.3	71.8	35.4	55.0	10.7	22.7	54.0	55.6	41.3	54.2	47.7	41.6
CIL	FCS	CVPR 2024	58.3	78.5	75.1	76.2	42.6	59.8	10.2	24.3	35.3	34.9	44.3	54.7	52.1	44.2
LReID	AKA	CVPR 2021	51.2	72.0	47.5	45.1	18.7	33.1	16.4	37.6	27.7	27.6	32.3	43.1	44.3	40.4
LReID	KRKC	AAAI 2023	60.2	83.6	84.0	86.3	58.9	76.0	24.2	51.5	43.1	44.3	54.1	68.5	59.4	53.0
LReID	MEGE	TPAMI 2023	39.0	61.6	73.3	76.6	16.9	30.3	4.6	13.4	36.4	37.1	34.0	43.8	47.7	44.0
LReID	ConRFL	PR 2023	59.2	78.3	82.1	84.3	45.6	61.8	12.6	30.4	51.7	53.8	50.2	61.7	57.4	52.3
LReID	CKP	MM 2024	53.8	76.0	81.2	83.0	49.7	67.0	18.4	40.8	44.1	45.8	49.4	62.5	58.0	51.0
LReID	LSTKC	AAAI 2024	54.7	76.0	81.1	83.4	49.4	66.2	20.0	43.2	44.7	46.5	50.0	63.1	57.0	49.9
LReID	DASK	AAAI 2025	61.2	82.3	81.9	83.7	58.5	74.6	29.1	57.6	46.2	48.1	55.4	69.3	65.3	58.4
	Ours	-	67.1	84.9	84.1	85.2	59.9	76.2	32.9	61.2	57.2	59.3	60.2	73.4	66.1	59.5

Table 3: Comparison of different methods on Training Order-2 with mAP and R1 scores.

	Method	Publication	DukeMTMC		MSMT17		Market-1501		CUHK-SYSU		CUHK03		Seen-Avg		UnSeen-Avg	
			mAP	R@1	mAP	R@1	mAP	R@1	mAP	R@1	mAP	R@1	mAP	R@1	mAP	R@1
	JointTrain	-	71.2	82.9	36.2	61.2	78.9	90.9	86.7	88.2	61.2	63.4	66.8	77.3	59.4	52.6
CIL	SPD	ICCV 2019	28.5	48.5	3.7	11.5	32.3	57.4	62.1	65.0	43.0	45.2	33.9	45.5	39.8	36.3
CIL	PRAKA	ICCV 2023	31.2	48.7	6.6	19.1	47.8	69.8	70.4	73.0	54.9	56.6	42.2	53.4	48.4	41.1
CIL	FCS	CVPR 2024	53.6	70.0	9.5	23.5	48.7	69.9	76.2	78.2	37.1	38.4	45.0	56.0	52.7	45.1
LReID	KRKC	AAAI 2023	50.1	68.6	17.7	41.1	69.0	88.3	85.2	87.4	40.4	41.6	52.5	65.4	59.4	53.4
LReID	MEGE	TPAMI 2023	21.6	35.5	3.0	9.3	25.0	49.8	69.9	73.1	34.7	35.1	30.8	40.6	44.3	41.1
LReID	CKP	MM 2024	49.4	67.0	14.5	33.8	56.0	77.6	83.2	84.9	45.3	47.1	49.7	62.1	57.2	50.0
LReID	LSTKC	AAAI 2024	49.9	67.6	14.6	34.0	55.1	76.7	82.3	83.8	46.3	48.1	49.6	62.1	57.6	49.6
LReID	DKP	CVPR 2024	53.4	70.5	14.5	33.3	60.6	81.0	83.0	84.9	45.0	46.1	51.3	63.2	59.0	51.6
LReID	DASK	AAAI 2025	55.7	74.4	25.2	51.9	71.6	87.7	84.8	86.2	48.4	49.8	57.1	70.0	65.5	57.9
	Ours	-	55.9	73.3	29.2	57.8	71.7	88.2	85.0	86.5	55.5	57.7	59.4	72.8	65.8	58.7

LReID methods (AKA [2], MEGE [20], ConRFL [49], CKP [50], LSTKC [4] and DASK [5]). In addition, we evaluate Joint Training, which leverages all available data from seen domains and serves as an upper bound for LReID methods. For fair comparison, all methods are implemented following their official publications and evaluated under the same backbone and training settings.

We first present the evaluation results on Training Order-1 and Order-2 in Tables 2 and 3, respectively. As observed, our method consistently outperforms traditional CIL methods, replay-based LReID approaches, and exemplar-free methods by a significant margin. Specifically, across both training orders, it achieves average improvements of +15.2%/+17.8%, +6.5%/+6.2%, and +3.6%/+3.5% in Seen-Avg mAP/R@1 over the best-performing baselines in each respective category. Notably, our approach maintains highly stable performance regardless of the domain sequence, yielding Seen-Avg mAP/R@1 scores of around 60%/73%. We attribute this robust stability to our proposed **Information-Dense Replay** and **Bidirectional Style-Semantic Alignment**. By condensing diverse historical knowledge into a compact buffer, the model effectively preserves rich fine-grained semantics to mitigate forgetting. Furthermore, this dense retention of past knowledge does not compromise the model's plasticity for new tasks. For instance, our method achieves a remarkable +9.1%/+9.6% improvement in mAP/R@1 on the CUHK03 dataset, demonstrating an optimal balance between retaining old knowledge and adapting to new domains.

To further analyze the learning dynamics, we visualize the per-domain and overall average mAP trends under Training Order-1 in Figure 4. While

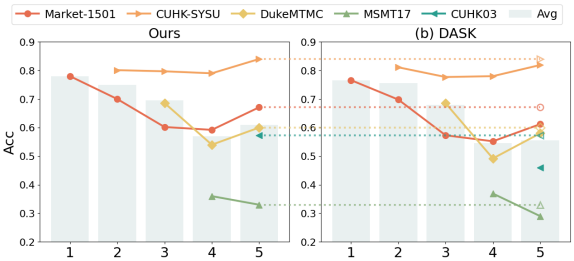

Fig. 4: Accuracy tendency on each domain and overall average trend across training stages.

most methods exhibit comparable accuracy during the initial stages, our approach demonstrates significantly stronger resistance to catastrophic forgetting as the training sequence progresses, maintaining a clear performance lead across all historical domains in the later stages. This empirical trend consistently aligns with the quantitative results in Table 2, particularly highlighting our method's superior plasticity on new tasks (e.g., the substantial mAP surge on CUHK03 at Stage 5). These observations confirm that breaking the physical memory bottleneck via multi-stage condensation allows the network to continuously absorb new information without overwriting critical past semantics.

Beyond mitigating forgetting on seen domains, our method exhibits exceptional cross-domain generalization. It improves Seen-Avg performance by over 5% compared to the strongest baseline while simultaneously achieving comparable or superior results on Unseen-Avg metrics. Remarkably, when compared to Joint Training, which accesses all data simultaneously and serves as the theoretical upper bound, our method achieves an overall average mAP/R@1 of 63.2%/66.5% across all twelve domains (both seen and unseen), essentially matching the 63.1%/65.0% achieved by Joint Training. This indicates that despite relying on a condensed replay buffer, our model does not overfit to historical data. Instead, the bidirectional style-semantic alignment effectively harmonizes feature representations, enabling robust generalization to entirely unseen distributions. Ultimately, our framework matches the upper bound of joint training while strictly adhering to sequential learning and data privacy constraints, establishing a highly efficient and robust new baseline for LReID.

Table 4: Ablation on Condense and Replay components.

Condense			Data R	BSSA	Seen-Avg		UnSeen-Avg	
GM	ID	Loss			mAP	R@1	mAP	R@1
			✓		54.1	69.3	57.1	52.5
✓			✓		57.9	73.3	61.2	56.4
	✓		✓		55.8	71.1	58.5	54.2
✓	✓		✓		58.7	72.0	62.9	57.1
✓	✓		✓	✓	60.2	73.4	66.1	59.5

5.4 Ablation Study

To validate the effectiveness of our proposed components, we present a detailed ablation study in Table 4. Here, the "Data R" baseline denotes the traditional LReID approach that relies solely on standard raw image replay.

As observed, progressively incorporating our multi-stage gradient matching and ID supervision yields substantial performance gains over the baseline. Specifically, replacing sparse raw images with synthetic samples significantly maximizes the information density of the limited memory buffer, allowing it to encapsulate richer historical training dynamics. Furthermore, integrating the ID loss explicitly forces the highly condensed pixels to retain fine-grained, class-discriminative semantics, effectively preventing the feature collapse that often occurs during pure trajectory matching.

Finally, applying the Bidirectional Style-Semantic Alignment on top of the condensed buffer further mitigates catastrophic forgetting. By bidirectionally exchanging styles between the current domain data and the historical replay samples, this strategy harmonizes feature representations across disparate domains. This not only neutralizes the negative impact of severe cross-domain shifts but also enriches the stylistic diversity of the training data, thereby notably improving the model's overall generalization performance.

6 Parameter Analysis

6.1 Condensation Parameter Analysis

We show the influence of the gradient matching weight α in Figure 5(a). Within a proper variation range, the performance remains stable. However,

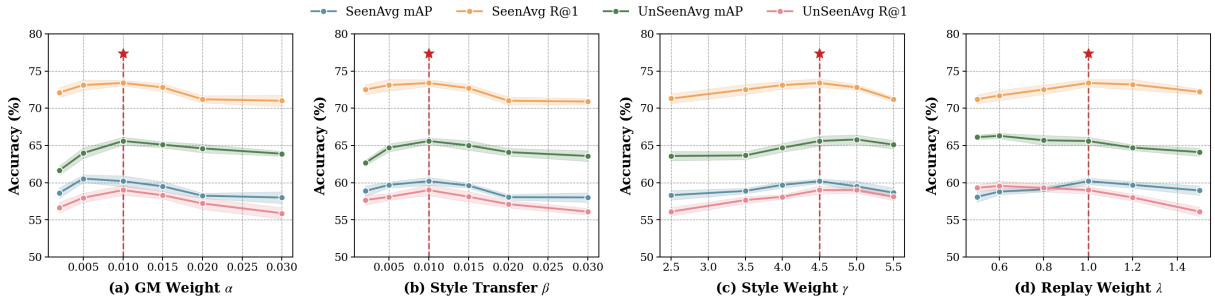

Fig. 5: Hyper-parameter analysis of our framework: (a) Gradient matching loss weight (α); (b) Perceptual loss weight (β) for structural preservation; (c) Style alignment weight (γ); and (d) Information-dense replay weight (λ). Average performance over five independent runs on Training Order 1 is reported. Dashed lines indicate the default values adopted in our final model.

further increasing the gradient matching weight on the condensed samples diminishes the consideration of inter-class relationships, leading to performance degradation. This is particularly critical in ReID tasks, where the inter-class variance is relatively small. A consistent performance drop is observed when α reaches 0.02. Based on these observations, we set α to 0.01.

6.2 Style Reconstruction Weight Analysis

We present the influence of the style reconstruction weight β in Figure 5(b). It can be observed that the model performance initially improves and then degrades as the style reconstruction loss weight β increases. This is because introducing the style reconstruction loss encourages the model to better capture style-related information rather than solely focusing on pixel-level reconstruction. However, when β becomes too large, the model may overemphasize style consistency and neglect pixel-level fidelity, which undermines the realism of the transferred samples. Based on these observations, we set β to 0.01.

6.3 Replay Parameters Analysis

We investigate the impact of BSSA weight γ and the data replay weight λ in Figure 5(c) and Figure 5(d), respectively. As γ increases, the performance improves on both seen and unseen domains. This is because BSSA allows the model to observe past-domain styles applied to current-domain data, as well as past data adapted to the current domain style. This enhances both forgetting resistance and style diversity during training. However, continuously increasing the weight reduces the realism of the training distribution, which negatively affects performance. We observe that the performance on seen domains starts to drop when γ exceeds 5.0.

For λ, the performance remains stable within a moderate range. However, further increasing the diversity of the replayed data leads to reduced generalization, likely because the model pays less attention to newly arriving data when overfitting to the replayed samples. A consistent performance drop is observed when λ reaches 1.5. Based on these results, we set γ to 4.5 and λ to 1.0.

Table 5: Ablation study on the components of our Information-Dense Replay.

Replay	Mask	Condense	Seen-Avg mAP	Seen-Avg R@1	UnSeen-Avg mAP	UnSeen-Avg R@1
✓			54.1	69.3	57.1	52.5
✓	✓		52.9	68.2	57.3	52.6
✓		✓	59.3	72.6	63.4	57.5
✓	✓	✓	58.7	72.0	62.9	57.1

7 Module Effectiveness Analysis

7.1 Privacy Analysis

7.1.1 Privacy Definition and Performance Context

In the context of person Re-ID, training datasets fundamentally consist of surveillance images of

real pedestrians. The unauthorized retention of such raw biometric data within memory buffers poses a significant risk of portrait rights infringement. Therefore, a practical LReID system must prevent the leakage of sensitive identity information.To establish a fundamental baseline for privacy protection, our framework explicitly applies Gaussian blur to predefined facial regions prior to the condensation process. As observed in Table 5, incorporating face masking leads to only a marginal performance drop (1%), while the domain-generalization performance remains largely unaffected. This observation aligns with existing literature [51], which suggests that Re-ID models rely predominantly on holistic body cues, such as clothing, posture, and body shape, rather than high-frequency facial details. Consequently, obscuring the face effectively mitigates the risk of identity exposure without compromising the model's feature-extraction capabilities.

7.1.2 Threat Model Definition

Since privacy protection acts as an intrinsic benefit of our condensation framework rather than its primary goal, we focus on two prevalent vulnerabilities in replay-based LReID: Data Reconstruction and MIA. We assume a strict white-box threat model where the adversary is defined as a compromised server with unconstrained access to the continual learning system.

Attacker Capabilities: The adversary possesses full access to the current model parameters θ_t and the entire auxiliary replay buffer $\mathcal{S}$ containing the condensed samples $\tilde{x}_m$.

Attacker Objectives: Utilizing the accessible θ_t and $\mathcal{S}$, the adversary has two primary objectives: (1) Data Reconstruction, attempting to computationally invert $\tilde{x}_m$ to visually recover sensitive biometric identifiers of the original pedestrians; and (2) Membership Inference Attack (MIA), deducing whether a specific raw image x_i was utilized in the condensation process, thereby exposing the individual's presence in the historical data.

7.1.3 Theoretical Analysis

Despite the attacker's full knowledge of θ_t and $\mathcal{S}$, reversing the condensation process mathematically constitutes an extreme, ill-posed inverse problem.During our information-dense condensation, a batch of N distinct raw images $\{x_1, ..., x_N\}$

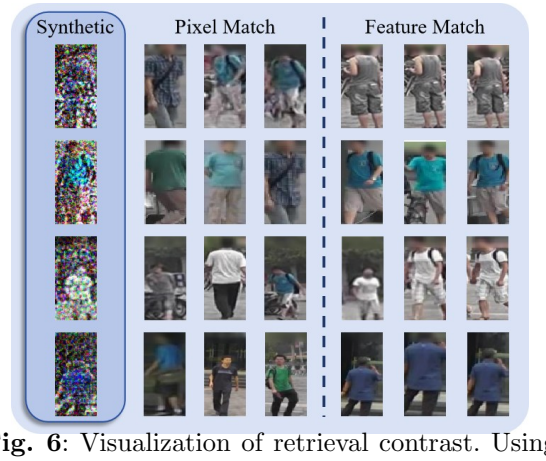

Fig. 6: Visualization of retrieval contrast. Using a condensed image as a query, pixel-level retrieval fails (yielding incorrect identities), while feature-level retrieval successfully matches the correct original identities, demonstrating visual anonymity.

of the same identity is condensed into a single synthetic representation $\tilde{x}_m$ by matching their mean gradient trajectory (as defined in Eq. 7):

$$\nabla_\theta \mathcal{L}^{\mathcal{S}}(\tilde{x}_m) \approx \frac{1}{N} \sum_{i=1}^{N} \nabla_\theta \mathcal{L}^{\mathcal{T}}(x_i) \tag{14}$$

For a white-box attacker to reconstruct a specific x_i from $\tilde{x}_m$, they must invert a many-to-one mapping through the highly non-linear, high-dimensional space of the Re-ID network ϕ_θ. Because the neural network acts as a highly non-linear dimensionality reduction function, inverting the averaged gradient back to N distinct pixel spaces mathematically yields infinite possible solutions.Furthermore, the identity supervision ($\mathcal{L}_c + \mathcal{L}_t$) applied during condensation strictly enforces semantic separability in the feature space rather than fidelity in the pixel space. Combined with our prior region-wise facial masking, the optimized $\tilde{x}_m$ collapses into a "hybrid artifact." It successfully aggregates generic identity-discriminative cues (e.g., clothing color) while irreversibly destroying instance-specific biometric identifiers.

7.1.4 Empirical Assessment

To validate our theoretical defense against the defined white-box adversary, we empirically evaluate the condensed buffer $\mathcal{S}$, demonstrating a strict decoupling of semantic identity from visual fidelity.

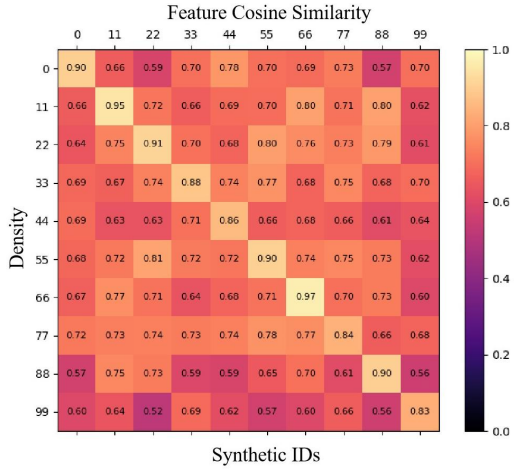

Fig. 7: Feature cosine similarity matrix between synthetic queries and real identities. The distinctly high values along the diagonal confirm that the condensed space preserves strict semantic separability.

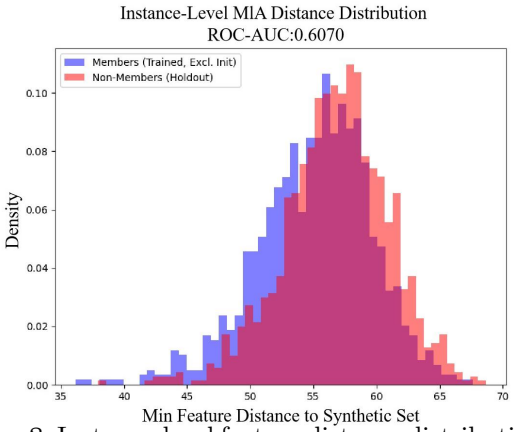

Fig. 8: Instance-level feature distance distribution of member (training) and non-member (holdout) samples to the synthetic set. The highly overlapping distributions highlight the model's resistance to Membership Inference Attacks.

Visual Anonymity via Representation Decoupling. Visually, the synthesized samples manifest as uninterpretable, high-frequency noise (see Figure 6). We rigorously validate this anonymity through a retrieval task: when utilizing a condensed image as a query, pixel-level retrieval (via Euclidean distance) completely fails to locate the correct original identities. Conversely, feature-level retrieval (via cosine similarity extracted by θ_t) successfully matches them. This confirms that $\mathcal{S}$ perfectly encapsulates structural identity knowledge in the deep feature space while permanently destroying pixel-level biometric data.

Table 6: Performance comparison of different strategies on three person re-identification benchmarks. Each method uses only two samples per class.

Method	Market-1501	CUHK-SYSU	DukeMTMC
Full	78.9	86.7	71.2
Random	72.3	76.8	65.9
K-center	75.2	79.1	68.5
Ours	78.8	82.5	71.0

Semantic Integrity of the Condensed Space. Despite extreme visual distortion, the condensed samples retain strict inter-class separability. As illustrated in Figure 7, the feature cosine similarity matrix between synthetic queries and real IDs is distinctly diagonal; synthetic samples yield strong feature activations exclusively with their corresponding real classes. This indicates that the identity supervision applied during condensation successfully preserves the pristine classification boundaries required for Re-ID without compromising privacy.

Resistance to MIA. We evaluate white-box MIA vulnerability by computing the minimum feature distance from both member (training) and non-member (holdout) samples to the synthetic set. As shown in Figure 8, the resulting instance-level distance distributions are heavily intertwined and nearly indistinguishable. Quantitatively, the MIA ROC-AUC score is 0.6153, remarkably close to random chance (0.5) and significantly lower than the $> 85\%$ success rate typical of raw image buffers. This confirms that our multi-to-one gradient fusion intrinsically obfuscates individual membership traces, rendering MIA mathematically intractable.

7.2 Validation of the Condensation Mechanism

In this section, we conduct an ablation study from a different perspective to evaluate the effectiveness of our proposed condensation strategy. Specifically, we compare three sampling approaches on the Market1501 [32], CUHK-SYSU [34] and DukeMTMC [33] benchmarks: random selection,

Table 7: Comparison of different methods on Training Order-1 with mAP and R1 scores. Best results are highlighted in deep lavender and second best in light lavender. † indicates results with data replay only, excluding style replay.

	Method	Publication	Market-1501		CUHK-SYSU		DukeMTMC		MSMT17		CUHK03		Seen-Avg		UnSeen-Avg	
			mAP	R@1	mAP	R@1	mAP	R@1	mAP	R@1	mAP	R@1	mAP	R@1	mAP	R@1
	JointTrain	-	78.9	90.9	86.7	88.2	71.2	82.9	36.2	61.2	61.2	63.4	66.8	77.3	59.4	52.6
Replay	GwFReID	AAAI 2021	57.7	77.4	79.6	81.7	48.5	66.4	22.0	45.0	58.8	61.4	53.3	66.4	51.4	44.9
Replay	PTKP	AAAI 2022	73.5	88.0	84.8	86.6	59.0	75.0	23.2	47.1	51.6	53.8	58.4	70.1	57.5	51.1
Replay	KRKC	AAAI 2023	60.2	83.6	84.0	86.3	58.9	76.0	24.2	51.5	43.1	44.3	54.1	68.5	59.4	53.0
Replay	Ours†	-	66.5	84.0	84.2	85.5	59.6	75.1	32.3	59.9	56.8	58.5	58.7	72.0	62.9	57.1

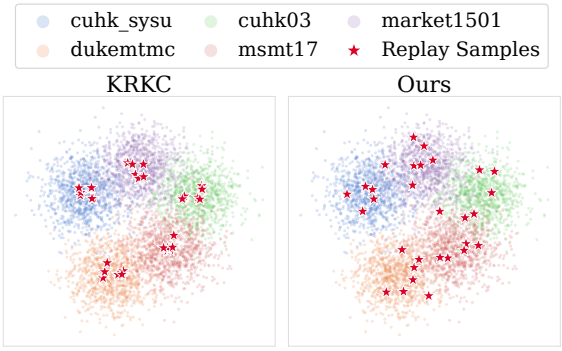

Fig. 9: t-SNE of replay features under Training Order 1 for KRKC and Ours.

clustering-based selection, and our method. For each method, we retain two samples per class and use them to train the model.

The detailed results are presented in Table 6. Remarkably, our proposed method achieves performance comparable to training with the full dataset on both the Market-1501 and DukeMTMC benchmarks. On CUHK-SYSU, it also outperforms both the random and K-center selection strategies by a noticeable margin. This shows that, under the same memory budget, our approach enables the replay buffer to preserve more diverse and informative samples, leading to improved model performance. These results highlight the efficiency of our strategy in utilizing limited memory for LReID.

7.3 Data Replay Analysis

Existing replay-based LReID methods typically construct their memory buffer by selecting a few raw images closest to the feature center of each identity. While this simple heuristic ensures basic representativeness, it fundamentally severely restricts sample diversity. Because each limited memory slot is occupied by a single, discrete raw image, the physical memory budget is highly underutilized, leaving the vast majority of crucial intra-class variance discarded.

In contrast, our approach transcends discrete sample selection. Rather than passively storing isolated raw images, we dynamically condense the knowledge of entire data sequences into synthetic representations. By leveraging our multi-stage gradient matching strategy, we fuse the diverse intra-class variations of multiple real samples into a single, optimized image. Consequently, each stored sample in our buffer is no longer a sparse instance, but a highly information-dense composite that maximizes the semantic capacity of the memory space.

To empirically validate this advantage, we visualize the t-SNE feature distributions of the replay buffers generated by the KRKC baseline and our proposed method in Figure 9. As illustrated, while KRKC's discrete selection captures the central high-density regions, it inevitably leaves the broader data distribution unrepresented due to memory limits. Conversely, our synthesized samples exhibit a much more comprehensive coverage of the entire identity embedding space, effectively capturing both high-density cores and low-density boundary variations. By providing a significantly richer and more accurate proxy for the global historical data distribution, our Information-Dense Replay intrinsically equips the model with stronger resistance to catastrophic forgetting.

To further evaluate the effectiveness of our condensation strategy, we isolate our Information-Dense Replay module and compare it against state-of-the-art replay-based baselines [3, 24, 52] in Tables 7 and 8. For a strictly fair comparison, our Bidirectional Style-Semantic Alignment is entirely disabled in this setting.

Table 8: Comparison of different methods on Training Order-2 with mAP and R1 scores.

	Method	Publication	DukeMTMC mAP	DukeMTMC R@1	MSMT17 mAP	MSMT17 R@1	Market-1501 mAP	Market-1501 R@1	CUHK-SYSU mAP	CUHK-SYSU R@1	CUHK03 mAP	CUHK03 R@1	Seen-Avg mAP	Seen-Avg R@1	UnSeen-Avg mAP	UnSeen-Avg R@1
	JointTrain	-	71.2	82.9	36.2	61.2	78.9	90.9	86.7	88.2	61.2	63.4	66.8	77.3	59.4	52.6
Replay	GwFReID	AAAI 2021	46.4	64.1	16.5	36.3	65.7	83.7	80.4	82.4	58.4	61.5	53.5	65.6	52.2	45.9
Replay	PTKP	AAAI 2022	58.6	74.3	16.4	37.3	67.1	84.8	83.1	85.1	49.8	52.9	55.0	66.9	57.5	51.1
Replay	KRKC	AAAI 2023	50.1	68.6	17.7	41.1	69.0	88.3	85.2	87.4	40.4	41.6	52.5	65.4	59.4	53.4
Replay	Ours†	-	55.2	72.9	28.7	56.8	70.8	87.4	84.9	86.3	55.0	57.2	58.8	72.0	63.3	56.8

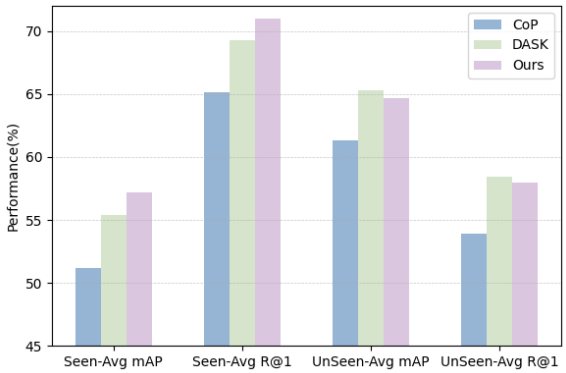

Fig. 10: Accuracy comparison under different style transfer.

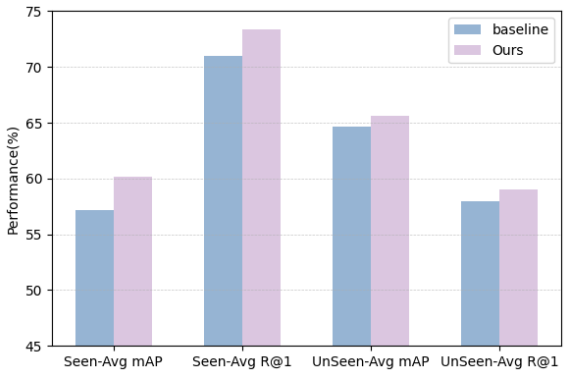

Fig. 11: Effectiveness of the proposed BSSA. We compare the performance with and without applying the style strategy to the information-dense replay samples.

As observed, under an identical memory budget, our multi-stage gradient matching approach consistently yields superior overall performance. While certain baselines may exhibit localized performance peaks on either the first (over-stability) or the recent domain (over-plasticity), our method demonstrates a significantly more balanced and robust accuracy across the entire domain sequence. We attribute this optimal balance to the drastically higher information density encapsulated within our synthetic samples. By breaking the constraint of storing discrete raw images, our condensed buffer provides a richer and more comprehensive semantic representation, allowing the model to acquire new information without aggressively overwriting past knowledge. Consequently, our approach fundamentally maximizes replay efficiency while intrinsically yielding data privacy as a natural by-product.

7.4 Bidirectional Style-Semantic Alignment Analysis

To evaluate the efficacy of our proposed BSSA, we first compare it against existing style transfer LReID methods, such as CoP and DASK, as shown in Figure 10. While these baselines attempt to mitigate domain shift by applying past-domain styles to current training data, they rely exclusively on pixel-level L1 reconstruction losses. As analyzed in our methodology, this inevitably blurs the high-frequency structural details (e.g., textures and edges) that are essential for fine-grained Re-ID. By introducing the Perceptual Integrity Safeguard, our method strictly preserves these critical structural semantics during stylization. Consequently, our approach achieves significantly improved performance on seen domains. While DASK exhibits slightly higher performance on completely unseen domains due to its aggressive abstract distribution blurring, our method deliberately prioritizes the strict preservation of structural identity. This strategic trade-off massively suppresses catastrophic forgetting on historical domains—the primary goal of LReID—while still maintaining highly competitive generalization capabilities.

Impact of Bidirectional Translation. During the replay phase, the model is trained jointly on current-domain samples and replay samples. However, a critical issue largely overlooked by traditional replay-based methods is that the replay

memory itself becomes a heterogeneous mixture of disparate historical domains. This severe internal domain discrepancy actively interferes with current-domain training. To overcome this, our BSSA employs a dual-translation process.

Instead of applying style transfer only to the current streaming data (as done in standard baselines), we concurrently inject the current-domain style into our information-dense replay samples. By bidirectionally aligning the styles, the network observes the identical identity semantics under multiple domain-specific appearances simultaneously. As demonstrated in Figure 11, the baseline (applying style transfer only to current data) leaves the replay samples stylistically misaligned, inherently limiting their replay effectiveness. By contrast, applying our dual-translation process strictly harmonizes the feature space across domains. This not only neutralizes the internal domain discrepancies within the replay buffer but also enriches the stylistic diversity of the highly condensed historical features, leading to consistent performance improvements and exceptionally robust resistance to cross-domain forgetting.

8 Conclusion

In this work, we address the critical challenges of memory constraints, catastrophic forgetting, and data privacy in LReID. To overcome these hurdles, we propose a novel Information-Dense and Style-Aware Replay framework. By shifting the paradigm from discrete image storage to continuous information condensation, our method successfully fuses the knowledge of sequential domains into a highly compact replay buffer. This pixel-level synthesis, combined with privacy-guided initialization, not only maximizes the representativeness of limited memory but also inherently conceals sensitive visual details, providing a natural safeguard for biometric privacy. Furthermore, to tackle the severe domain shifts inherent in LReID, we introduce a Bidirectional Style-Semantic Alignment strategy. By jointly harmonizing the styles of both current streaming data and fused replay samples while strictly preserving high-frequency structural identities, our model effectively neutralizes cross-domain forgetting.

Extensive experiments demonstrate that our approach achieves state-of-the-art performance across various training trajectories. More importantly, by eliminating the necessity to store raw pedestrian images, our framework resolves a fundamental privacy bottleneck, clearing a major roadblock for the real-world deployment of replay-based LReID systems. We hope this work can serve as a robust new baseline and inspire future research in two promising directions: exploring advanced information fusion techniques for Re-ID, and developing inherently privacy-friendly architectures for continual learning.

Acknowledgments

This work was supported by the Zhejiang Province Natural Science Foundation of China [Grant Z24F030004] and the National Natural Science Foundation of China [Grant 62173302].

References

[1] Dai, Y., Sun, Y., Liu, J., Tong, Z., Duan, L.-Y.: Bridging the source-to-target gap for cross-domain person re-identification with intermediate domains. International Journal of Computer Vision **133**(1), 410–434 (2025)

[2] Pu, N., Chen, W., Liu, Y., Bakker, E.M., Lew, M.S.: Lifelong person re-identification via adaptive knowledge accumulation. In: 2021 IEEE/CVF Conference on Computer Vision and Pattern Recognition (CVPR), pp. 7897–7906 (2021). https://doi.org/10.1109/CVPR46437.2021.00781

[3] Yu, C., Shi, Y., Liu, Z., Gao, S., Wang, J.: Lifelong person re-identification via knowledge refreshing and consolidation. Proceedings of the AAAI Conference on Artificial Intelligence **37**(3), 3295–3303 (2023) https://doi.org/10.1609/aaai.v37i3.25436

[4] Xu, K., Zou, X., Zhou, J.: Lstkc: Long short-term knowledge consolidation for lifelong person re-identification. Proceedings of the AAAI Conference on Artificial Intelligence **38**(14), 16202–16210 (2024) https://doi.org/10.1609/aaai.v38i14.29554

[5] Xu, K., Jiang, C., Xiong, P., Peng, Y., Zhou,

J.: Dask: Distribution rehearsing via adaptive style kernel learning for exemplar-free lifelong person re-identification. Proceedings of the AAAI Conference on Artificial Intelligence **39**(9), 8915–8923 (2025) https://doi.org/10.1609/aaai.v39i9.32964

[6] Ye, M., Shen, J., Lin, G., Xiang, T., Shao, L., Hoi, S.C.H.: Deep learning for person re-identification: A survey and outlook. IEEE Transactions on Pattern Analysis and Machine Intelligence **44**(6), 2872–2893 (2022) https://doi.org/10.1109/TPAMI.2021.3054775

[7] Luo, H., Jiang, W., Gu, Y., Liu, F., Liao, X., Lai, S., Gu, J.: A strong baseline and batch normalization neck for deep person re-identification. IEEE Transactions on Multimedia **22**(10), 2597–2609 (2020) https://doi.org/10.1109/TMM.2019.2958756

[8] Ye, M., Yuen, P.C.: Purifynet: A robust person re-identification model with noisy labels. IEEE Transactions on Information Forensics and Security **15**, 2655–2666 (2020) https://doi.org/10.1109/TIFS.2020.2970590

[9] Leng, J., Kuang, C., Li, S., Gan, J., Chen, H., Gao, X.: Dual-space video person re-identification. International Journal of Computer Vision **133**(6), 3667–3688 (2025)

[10] Zhang, X., Han, R., Wang, L., Song, L., Hou, J., Feng, W.: Synthetic-to-real video person re-id. IEEE Transactions on Information Forensics and Security **20**, 5438–5450 (2025) https://doi.org/10.1109/TIFS.2025.3574972

[11] Du, Y., Lei, C., Zhao, Z., Dong, Y., Su, F.: Video-based visible-infrared person re-identification with auxiliary samples. IEEE Transactions on Information Forensics and Security **19**, 1313–1325 (2024) https://doi.org/10.1109/TIFS.2023.3337972

[12] Zhang, Y., Yan, Y., Lu, Y., Wang, H.: Adaptive middle modality alignment learning for visible-infrared person re-identification. International Journal of Computer Vision **133**(4), 2176–2196 (2025)

[13] Zhang, T., Zhao, Y., Wang, L., Li, J.: Free lunch to meet the gap: Intermediate domain reconstruction for cross-domain few-shot learning. International Journal of Computer Vision **133**(8), 5118–5137 (2025)

[14] Zhang, L., Fu, X., Huang, F., Yang, Y., Gao, X.: An open-world, diverse, cross-spatial-temporal benchmark for dynamic wild person re-identification. International Journal of Computer Vision **132**(9), 3823–3846 (2024)

[15] Zhang, A., Wu, J., Gao, Y., Gao, M., Chen, Z., Song, Y., Pun, S.H.: Layered semi-second-order information bottleneck and auxiliary domain classification for person re-identification: A. zhang et al. International Journal of Computer Vision **133**(11), 7794–7816 (2025)

[16] Sun, J., Li, Y., Chen, L., Chen, H., Wang, M.: Dualistic disentangled meta-learning model for generalizable person re-identification. IEEE Transactions on Information Forensics and Security **20**, 1106–1118 (2025) https://doi.org/10.1109/TIFS.2024.3516540

[17] Ye, M., Shen, W., Zhang, J., Yang, Y., Du, B.: Securereid: Privacy-preserving anonymization for person re-identification. IEEE Transactions on Information Forensics and Security **19**, 2840–2853 (2024) https://doi.org/10.1109/TIFS.2024.3356233

[18] Mai, G., Cao, K., Lan, X., Yuen, P.C.: Secureface: Face template protection. IEEE Transactions on Information Forensics and Security **16**, 262–277 (2021) https://doi.org/10.1109/TIFS.2020.3009590

[19] Li, Q., Xu, K., Peng, Y., Zhou, J.: Exemplar-free lifelong person re-identification via prompt-guided adaptive knowledge consolidation. International Journal of Computer Vision **132**(11), 4850–4865 (2024)

[20] Pu, N., Zhong, Z., Sebe, N., Lew, M.S.: A memorizing and generalizing framework for lifelong person re-identification. IEEE Transactions on Pattern Analysis and Machine Intelligence **45**(11), 13567–13585 (2023) https://doi.org/10.1109/TPAMI.

2023.3297058

[21] Cui, Z., Zhou, J., Wang, X., Zhu, M., Peng, Y.: Learning continual compatible representation for re-indexing free lifelong person re-identification. In: 2024 IEEE/CVF Conference on Computer Vision and Pattern Recognition (CVPR), pp. 16614–16623 (2024). https://doi.org/10.1109/CVPR52733.2024.01572

[22] Sun, Z., MU, Y.: Patch-based knowledge distillation for lifelong person re-identification. In: Proceedings of the 30th ACM International Conference on Multimedia, pp. 696–707 (2022). https://doi.org/10.1145/3503161.3548179

[23] Gu, J., Luo, H., Wang, K., Jiang, W., You, Y., Zhao, J.: Color Prompting for Data-Free Continual Unsupervised Domain Adaptive Person Re-Identification (2023). https://doi.org/10.48550/ARXIV.2308.10716

[24] Ge, W., Du, J., Wu, A., Xian, Y., Yan, K., Huang, F., Zheng, W.-S.: Lifelong person re-identification by pseudo task knowledge preservation. Proceedings of the AAAI Conference on Artificial Intelligence **36**(1), 688–696 (2022) https://doi.org/10.1609/aaai.v36i1.19949

[25] Zhang, J., Chen, Z., Dai, L., Li, P., Sheng, B.: Gradient amplification for gradient matching based dataset distillation. Neural Networks **191**, 107819 (2025) https://doi.org/10.1016/j.neunet.2025.107819

[26] Vahidian, S., Wang, M., Gu, J., Kungurtsev, V., Jiang, W., Chen, Y.: Group distributionally robust dataset distillation with risk minimization. In: International Conference on Learning Representations (2025)

[27] Zhao, B., Bilen, H.: Dataset condensation with distribution matching. In: 2023 IEEE/CVF Winter Conference on Applications of Computer Vision (WACV), pp. 6503–6512 (2023). https://doi.org/10.1109/WACV56688.2023.00645

[28] Li, G., Togo, R., Ogawa, T., Haseyama, M.: Importance-aware adaptive dataset distillation. Neural Networks **172**, 106154 (2024) https://doi.org/10.1016/j.neunet.2024.106154

[29] Gu, J., Wang, K., Jiang, W., You, Y.: Summarizing stream data for memory-constrained online continual learning. Proceedings of the AAAI Conference on Artificial Intelligence **38**(11), 12217–12225 (2024) https://doi.org/10.1609/aaai.v38i11.29111

[30] Dong, T., Zhao, B., Lyu, L.: Privacy for free: How does dataset condensation help privacy? In: International Conference on Machine Learning, pp. 5378–5396 (2022). PMLR

[31] Chen, D., Kerkouche, R., Fritz, M.: Private set generation with discriminative information. In: Advances in Neural Information Processing Systems, vol. 35, pp. 14678–14690 (2022)

[32] Zheng, L., Shen, L., Tian, L., Wang, S., Wang, J., Tian, Q.: Scalable person re-identification: A benchmark. In: 2015 IEEE International Conference on Computer Vision (ICCV), pp. 1116–1124 (2015). https://doi.org/10.1109/ICCV.2015.133

[33] Ristani, E., Solera, F., Zou, R., Cucchiara, R., Tomasi, C.: Performance measures and a data set for multi-target, multi-camera tracking. In: European Conference on Computer Vision, pp. 17–35 (2016). https://doi.org/10.1007/978-3-319-48881-3_2 . Springer

[34] Xiao, T., Li, S., Wang, B., Lin, L., Wang, X.: End-to-end deep learning for person search. arXiv preprint arXiv:1604.01850 **abs/1604.01850** (2016) 1604.01850

[35] Wei, L., Zhang, S., Gao, W., Tian, Q.: Person transfer gan to bridge domain gap for person re-identification. In: 2018 IEEE/CVF Conference on Computer Vision and Pattern Recognition, pp. 79–88 (2018). https://doi.org/10.1109/CVPR.2018.00016

[36] Li, W., Zhao, R., Xiao, T., Wang, X.: Deepreid: Deep filter pairing neural network for

person re-identification. In: 2014 IEEE Conference on Computer Vision and Pattern Recognition, pp. 152–159 (2014). https://doi.org/10.1109/CVPR.2014.27

[37] Li, W., Zhao, R., Wang, X.: Human reidentification with transferred metric learning. In: Asian Conference on Computer Vision, pp. 31–44 (2012). https://doi.org/10.1007/978-3-642-37331-2_3 . Springer

[38] Li, W., Wang, X.: Locally aligned feature transforms across views. In: 2013 IEEE Conference on Computer Vision and Pattern Recognition, pp. 3594–3601 (2013). https://doi.org/10.1109/CVPR.2013.461

[39] Gray, D., Tao, H.: Viewpoint invariant pedestrian recognition with an ensemble of localized features. In: European Conference on Computer Vision, pp. 262–275 (2008). https://doi.org/10.1007/978-3-540-88682-2_21 . Springer

[40] Hirzer, M., Beleznai, C., Roth, P.M., Bischof, H.: Person re-identification by descriptive and discriminative classification. In: Scandinavian Conference on Image Analysis, pp. 91–102 (2011). https://doi.org/10.1007/978-3-642-21227-7_9 . Springer

[41] Wang, T., Gong, S., Zhu, X., Wang, S.: Person re-identification by video ranking. In: European Conference on Computer Vision, pp. 688–703 (2014). https://doi.org/10.1007/978-3-319-10593-2_45 . Springer

[42] Loy, C.C., Xiang, T., Gong, S.: Multi-camera activity correlation analysis. In: 2009 IEEE Conference on Computer Vision and Pattern Recognition, pp. 1988–1995 (2009). https://doi.org/10.1109/CVPR.2009.5206827

[43] Zhao, H., Tian, M., Sun, S., Shao, J., Yan, J., Yi, S., Wang, X., Tang, X.: Spindle net: Person re-identification with human body region guided feature decomposition and fusion. In: 2017 IEEE Conference on Computer Vision and Pattern Recognition (CVPR), pp. 907–915 (2017). https://doi.org/10.1109/CVPR.2017.103

[44] Howard, A., Sandler, M., Chen, B., Wang, W., Chen, L.-C., Tan, M., Chu, G., Vasudevan, V., Zhu, Y., Pang, R., Adam, H., Le, Q.: Searching for mobilenetv3. In: 2019 IEEE/CVF International Conference on Computer Vision (ICCV), pp. 1314–1324 (2019). https://doi.org/10.1109/ICCV.2019.00140

[45] Li, Z., Hoiem, D.: Learning without forgetting. IEEE Transactions on Pattern Analysis and Machine Intelligence **40**(12), 2935–2947 (2018) https://doi.org/10.1109/TPAMI.2017.2773081

[46] Tung, F., Mori, G.: Similarity-preserving knowledge distillation. In: 2019 IEEE/CVF International Conference on Computer Vision (ICCV), pp. 1365–1374 (2019). https://doi.org/10.1109/ICCV.2019.00145

[47] Shi, W., Ye, M.: Prototype reminiscence and augmented asymmetric knowledge aggregation for non-exemplar class-incremental learning. In: 2023 IEEE/CVF International Conference on Computer Vision (ICCV), pp. 1772–1781 (2023). https://doi.org/10.1109/ICCV51070.2023.00170

[48] Li, Q., Peng, Y., Zhou, J.: Fcs: Feature calibration and separation for non-exemplar class incremental learning. In: 2024 IEEE/CVF Conference on Computer Vision and Pattern Recognition (CVPR), pp. 28495–28504 (2024). https://doi.org/10.1109/CVPR52733.2024.02692

[49] Huang, J., Yu, X., An, D., Wei, Y., Bai, X., Zheng, J., Wang, C., Zhou, J.: Learning consistent region features for lifelong person re-identification. Pattern Recognition **144**, 109837 (2023) https://doi.org/10.1016/j.patcog.2023.109837

[50] Xu, K., Zhang, H., Li, Y., Peng, Y., Zhou, J.: Mitigate catastrophic remembering via continual knowledge purification for noisy lifelong person re-identification. In: Proceedings of the 32nd ACM International Conference on Multimedia, pp. 5790–5799 (2024). https://doi.org/10.1145/3664647.3681235

[51] Dietlmeier, J., Antony, J., McGuinness, K., O'Connor, N.E.: How important are faces for person re-identification? In: 2020 25th International Conference on Pattern Recognition (ICPR), pp. 6912–6919 (2021). https://doi.org/10.1109/ICPR48806.2021.9412340

[52] Wu, G., Gong, S.: Generalising without forgetting for lifelong person re-identification. Proceedings of the AAAI Conference on Artificial Intelligence **35**(4), 2889–2897 (2021) https://doi.org/10.1609/aaai.v35i4.16395